



## Calcium-responsive paramagnetic CEST agents

Goran Angelovski<sup>a,\*</sup>, Thomas Chauvin<sup>b</sup>, Rolf Pohmann<sup>c</sup>, Nikos K. Logothetis<sup>a,d</sup>, Éva Tóth<sup>b,\*</sup>

<sup>a</sup> Physiology of Cognitive Processes, Max Planck Institute for Biological Cybernetics, Spemannstr. 38, 72076 Tübingen, Germany

<sup>b</sup> Centre de Biophysique Moléculaire, CNRS, rue Charles Sadron, 45071 Orléans, France

<sup>c</sup> High-Field Magnetic Resonance Center, Max Planck Institute for Biological Cybernetics, Spemannstr. 38, 72076 Tübingen, Germany

<sup>d</sup> Imaging Science and Biomedical Engineering, University of Manchester, Oxford Road, Manchester M13 9PT, UK

### ARTICLE INFO

#### Article history:

Available online 15 July 2010

#### Keywords:

MRI  
PARACEST  
Molecular imaging  
Calcium sensitive  
Proton exchange

### ABSTRACT

The assessment of changes in the extracellular calcium concentration by magnetic resonance imaging would be a valuable biomedical research tool to monitor brain neuronal activity. In this perspective, we report here the synthesis of novel ligands consisting of tetraamide and bisamide derivatives of cyclen, **L**<sup>1</sup> and **L**<sup>2</sup>, respectively, each bearing imino(diacetate) moieties for Ca<sup>2+</sup> binding. Yb<sup>3+</sup> and Eu<sup>3+</sup> complexes are investigated as chemical exchange saturation transfer (CEST) agents that respond to the presence of Ca<sup>2+</sup>. A CEST effect is observed for both **YbL**<sup>1</sup> and **EuL**<sup>1</sup> complexes ( $B = 11.7$  T), originating from the slow exchange of the amide protons and those of the coordinated water, respectively, whilst no CEST is detected for complexes of **L**<sup>2</sup>. Upon calcium binding, the CEST effect decreases considerably (from 60% to 20% for **YbL**<sup>1</sup> and from 35% to 10% for **EuL**<sup>1</sup>). A similar variation is observed in the presence of Mg<sup>2+</sup>. The affinity constants between the lanthanide complexes and the alkaline earth metal ions have been estimated from the variation of the CEST effect to be  $K_{\text{aff}}^{\text{YbL}^1-\text{Ca}} = 8 \pm 2 \text{ M}^{-1}$ ,  $K_{\text{aff}}^{\text{YbL}^1-\text{Mg}} = 23 \pm 3 \text{ M}^{-1}$  and  $K_{\text{aff}}^{\text{EuL}^1-\text{Ca}} = 10 \pm 3 \text{ M}^{-1}$ . These low values imply the coordination of the alkaline earth ions to a single iminodiacetate arm. Ca<sup>2+</sup>/Mg<sup>2+</sup> binding to the lanthanide complexes slows down the exchange of the amide protons on **YbL**<sup>1</sup> which is responsible for the diminished CEST effect. This has been evidenced by assessing the proton exchange rates from the dependency of the CEST effect on the saturation time and the saturation power, in the absence and in the presence of Ca<sup>2+</sup> and Mg<sup>2+</sup>. The applicability of the PARACEST MRI agents for Ca<sup>2+</sup> detection has been evaluated on a 16 T MRI scanner.

© 2010 Elsevier Ltd. All rights reserved.

### 1. Introduction

Calcium is one of the essential elements of the human body; it has few rivals in its importance. It plays a central role in the physiology and biochemistry of organisms and of the cell. Ca<sup>2+</sup> is important in signal transduction pathways (where it acts as a secondary messenger), in neurotransmitter release from neurons, contraction of all muscle cell types and fertilisation. Several enzymes require calcium as a co-factor. Extracellular calcium is also important for maintaining the potential difference across excitable cell membranes, as well as proper bone formation. Around 99% of the total calcium content in the body is found in the bone and calcified cartilage in the form of calcium phosphate and calcium sulphate. The rest of calcium is present within the extracellular and intracellular fluids. In a typical cell, the intracellular concentration of ionised calcium is roughly 100 nM, but can increase up to 10- to 100-fold during certain cellular functions. The Ca<sup>2+</sup> concentration in extra-

cellular fluids is orders of magnitude higher than the intracellular space; in mammalian body fluids, it is around 1.25 mM with minor variations.<sup>1</sup> The development of selective organic fluorescent probes has helped significantly in the understanding of the role of calcium in vivo.<sup>2</sup> However, a fundamental limitation of light-based microscope imaging techniques employing fluorochromes, is that they are restricted to transparent samples of a limited thickness because of light absorption and scattering.

Magnetic resonance imaging (MRI) provides a good alternative to light-based microscopy that can circumvent these limitations. The visualisation of Ca<sup>2+</sup> concentration and its variations in time by imaging techniques would be particularly interesting to assess neuronal signalling in the brain where Ca<sup>2+</sup> acts as an important secondary messenger.<sup>3</sup> Significant changes in Ca<sup>2+</sup> concentration take place during neuronal activity.<sup>4</sup> Tracking the dynamics of Ca<sup>2+</sup> concentration changes could thus contribute to the understanding of the basic aspects of neuronal regulation or to highlight the abnormalities in the diseased state.<sup>5</sup> Currently, the in vivo neuroimaging techniques used to study the activity of brain networks are based on blood-oxygen-level dependent (BOLD) functional MRI (fMRI). The BOLD technique indirectly measures neural activity by detecting changes in blood flow to brain regions with increased

\* Corresponding authors. Tel.: +49 7071 601 916; fax: +49 7071 601 919 (G.A.); tel.: +33 2 38 25 76 25; fax: +33 2 38 63 15 17 (E.T.).

E-mail addresses: [goran.angelovski@tuebingen.mpg.de](mailto:goran.angelovski@tuebingen.mpg.de) (G. Angelovski), [eva.jakabth@cnrs-orleans.fr](mailto:eva.jakabth@cnrs-orleans.fr) (Éva Tóth).

energy requirements. Given the vascular origin of the signal, BOLD has some inherent physiological limitations.<sup>5</sup>

The first contrast agent designed for sensing  $\text{Ca}^{2+}$  by MRI was based on a  $\text{Gd}^{3+}$  complex that showed approximately an 80% increase in water proton relaxivity in the presence of calcium ions, in the micromolar concentration range corresponding to the intracellular  $\text{Ca}^{2+}$  concentration.<sup>7</sup> Atanasijevic et al. reported a  $T_2$  agent based on the  $\text{Ca}^{2+}$  related aggregation of superparamagnetic iron nanoparticles and calmoduline, also with an MRI response in the intracellular concentration range.<sup>8</sup> The main limitation of this latter approach is the relatively long time course of the Ca-dependent aggregation (a few seconds) inhibiting the detection of fast Ca-concentration changes. The concentration of free extracellular  $\text{Ca}^{2+}$  is in the millimolar range and also drops up to 30–35% from the resting state during intense stimulation (typically from 1.2 to 0.8 mM).<sup>9</sup> Sensing  $\text{Ca}^{2+}$  changes at millimolar concentrations seems more appropriate for MRI applications, as this concentration range is more compatible with the relatively high amount of the magnetic imaging probe needed to detect contrast changes. Targeting extracellular  $\text{Ca}^{2+}$  also simplifies the chemical design, as additional requirements for cell internalisation can be neglected. A series of  $\text{Gd}^{3+}$  complexes have been reported as potential contrast agents to target the extracellular  $\text{Ca}^{2+}$ .<sup>10–13</sup> The most effective compounds showed a ~10% relaxivity change under biologically relevant conditions (in brain extracellular fluid, for a  $\text{Ca}^{2+}$  concentration change between 0.8 and 1.2 mM) with a high selectivity for  $\text{Ca}^{2+}$ .

Recently, a new class of contrast agents have emerged that produce an image based on chemical exchange dependent saturation transfer (CEST).<sup>14</sup> They are an attractive alternative to gadolinium-based  $T_1$  contrast agents which locally shorten the relaxation time of bulk water protons to generate contrast in MRI.<sup>15,16</sup> CEST agents possess a proton with a moderate to slow exchange rate with the bulk water. Selective saturation of the MR frequency of this proton, followed by exchange with the water, reduces the intensity of the bulk water MR signal. PARACEST agents include a paramagnetic lanthanide ion which considerably shifts the MR frequency of the exchangeable proton to facilitate selective detection.<sup>17–19</sup>

PARACEST agents can be particularly well adapted to the design of responsive probes, and more recently, various examples have been reported with selective response to enzymes,<sup>20,21</sup> metabolites,<sup>22,23</sup> metal ions,<sup>24</sup> pH<sup>25,26</sup> or temperature.<sup>27</sup> With the intention of detecting  $\text{Ca}^{2+}$  via the PARACEST effect, we have prepared two novel ligands ( $\text{L}^1$  and  $\text{L}^2$ , Chart 1) based on a DOTA-tetraamide or DOTA-bisamide chelating unit for lanthanide complexation that bear four or two iminodiacetate arms. DOTA-tetraamide ligands are known to form sufficiently stable complexes with trivalent lanthanide cations and such complexes have been those most frequently investigated for application as PARACEST agents. Though the thermodynamic stability of the DOTA-tetraamide lanthanide complexes is considerably lower than that of the tetracarboxylate analogues, their kinetic inertness is extremely high ensuring suffi-

cient safety for potential in vivo applications.<sup>28</sup> The iminodiacetate moieties are known to have an affinity for  $\text{Ca}^{2+}$ , but they do not have a specific selectivity towards  $\text{Ca}^{2+}$  in the presence of other endogenous metal ions such as  $\text{Cu}^{2+}$ ,  $\text{Zn}^{2+}$  or  $\text{Mg}^{2+}$ . However, the extracellular  $\text{Ca}^{2+}$  concentration is considerably higher than that of the other cations, thus we may expect that will not interfere significantly with the detection of calcium. We should note that the iminodiacetate units are not expected to interfere in the formation of the lanthanide complex; the lanthanide ion is coordinated by the four macrocyclic nitrogens and the four amide oxygens, with one water molecule completing the inner coordination sphere. Herein we describe a detailed study of the CEST properties of the complexes formed with  $\text{Yb}^{3+}$  and  $\text{Eu}^{3+}$  and their variation in the presence of divalent cations  $\text{Ca}^{2+}$  and  $\text{Mg}^{2+}$ . MRI CEST experiments showing the feasibility of  $\text{Ca}^{2+}$  detection on phantoms are also reported.

## 2. Results and discussion

### 2.1. Synthesis

The synthesis of the complexes  $\text{EuL}^1$  and  $\text{YbL}^1$  was achieved in five steps (Scheme 1). The first involved the tetraalkylation of the cyclen with *N*-Boc-*N'*-bromoacetylenediamine **1**<sup>29</sup> to give macrocycle **2**. The amino groups were deprotected after treatment of **2** in methanolic HCl, and further alkylation with *tert*-butyl bromoacetate was carried out without isolation of the intermediate amino product.<sup>30</sup> Finally, the octaester **3** was treated with formic acid to give the ligand  $\text{L}^1$ . Complexes  $\text{EuL}^1$  and  $\text{YbL}^1$  were prepared by mixing the ligands with the corresponding lanthanide chloride salts in aqueous solutions which were kept at neutral pH during the complexation.

The bisamide complexes were prepared according to Scheme 2. The synthesis started from the commercially available DO2AtBu (**4**). Due to the presence of the acid labile *tert*-butyl protective groups, the synthetic route for  $\text{L}^1$  was slightly modified. DO2AtBu was alkylated with two molecules of the benzyl 2-(2-bromoacetamido)ethylcarbamate **5**<sup>31</sup> to give **6**. The Cbz protective groups were removed upon the reduction with hydrogen (2.5 bar) in the presence of 10% Pd/C. The amine **7** was alkylated with *tert*-butyl bromoacetate to give the hexaester **8**. Finally, all *tert*-butyl groups were removed upon the treatment with formic acid to give ligand  $\text{L}^2$ , which on reaction with the appropriate lanthanide chloride salt produced  $\text{EuL}^2$  and  $\text{YbL}^2$ . All complexes were characterised by mass spectrometry and the appropriate isotope pattern distribution was recorded.

### 2.2. CEST properties

The magnitude of the magnetisation transfer to the bulk water, called the CEST effect, is usually calculated according to the following equation:

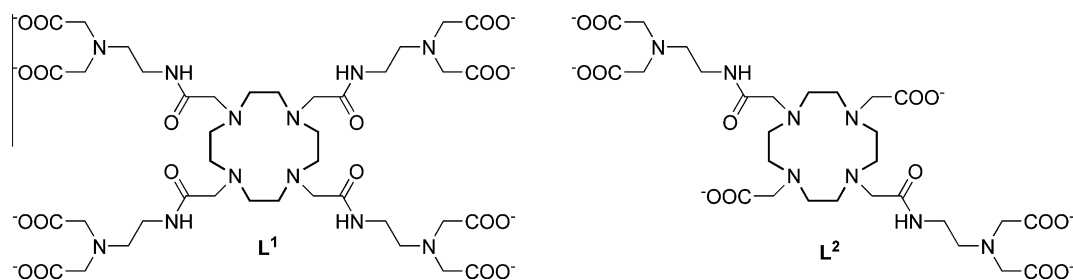
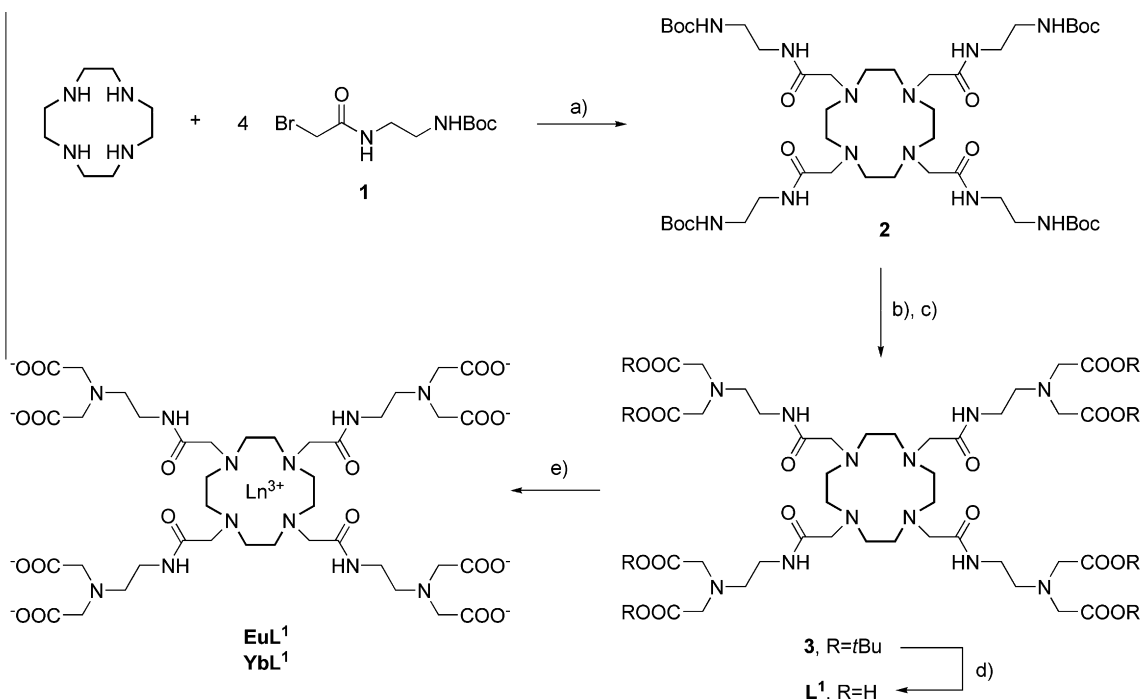
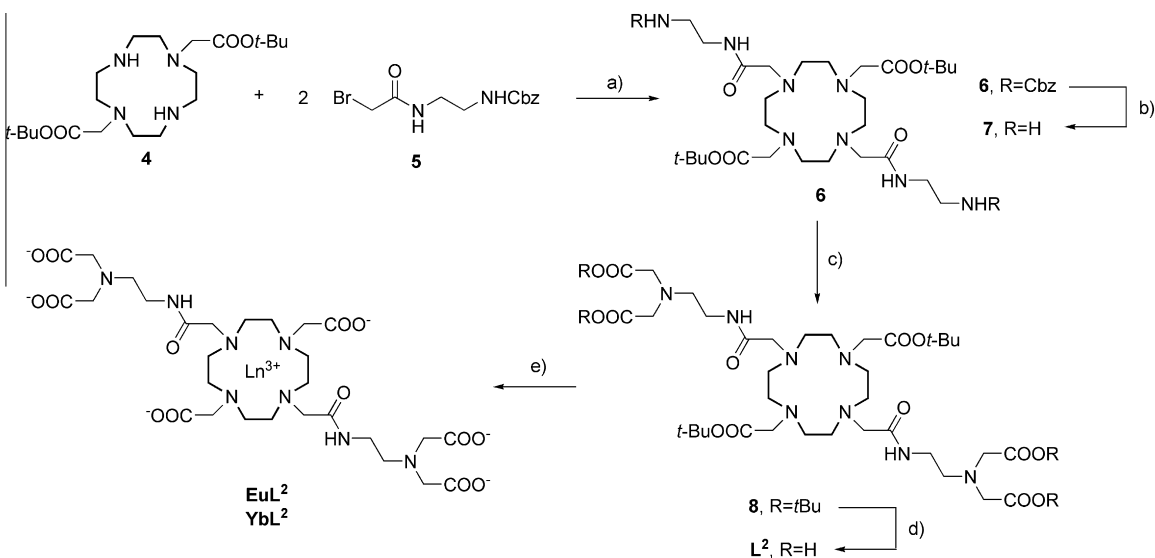


Chart 1. Structure of the ligands studied.



**Scheme 1.** Synthesis of **EuL<sup>1</sup>** and **YbL<sup>1</sup>**. Reagents and conditions: (a) K<sub>2</sub>CO<sub>3</sub>, CH<sub>3</sub>CN, 80 °C, 18 h. (b) HCl/CH<sub>3</sub>OH, 18 h. (c) *tert*-Butyl bromoacetate, K<sub>2</sub>CO<sub>3</sub>, CH<sub>3</sub>CN, 80 °C, 18 h. (d) HCOOH, 60 °C, 18 h. (e) EuCl<sub>3</sub> or YbCl<sub>3</sub>, H<sub>2</sub>O, 60 °C, 48 h.



**Scheme 2.** Synthesis of **EuL<sup>2</sup>** and **YbL<sup>2</sup>**. Reagents and conditions: (a) K<sub>2</sub>CO<sub>3</sub>, DMF, 24 h. (b) H<sub>2</sub>, Pd/C, CH<sub>3</sub>OH, 18 h. (c) *tert*-Butyl bromoacetate, K<sub>2</sub>CO<sub>3</sub>, CH<sub>3</sub>CN, 80 °C, 18 h. (d) HCOOH, 60 °C, 18 h. (e) EuCl<sub>3</sub> or YbCl<sub>3</sub>, H<sub>2</sub>O, 60 °C, 48 h.

$$\% \text{CEST} = (1 - M_s/M_0) \times 100\% \quad (1)$$

Here  $M_s$  is the intensity of the magnetic resonance signal of the bulk water taken after applying the radiofrequency (RF) saturation pulse at the resonance frequency of the exchangeable proton(s) of the contrast agent and  $M_0$  is the intensity of the reference signal, that is, recorded after applying the RF saturation pulse symmetrically on the opposite side of the bulk water signal, to correct for non-selective saturation, mostly direct water saturation. To visualise the magnetisation transfer, CEST spectra are typically used when the ratio of the solvent water signal intensities measured with and without presaturation ( $M_s/M_{\text{off}}$ ) is plotted against the presaturation frequency. Figure 1 shows the CEST spectra recorded for

**EuL<sup>1</sup>** and **YbL<sup>1</sup>**. The peak at 0 ppm represents direct saturation of bulk water. The peak centred at 41 ppm in the spectrum of **EuL<sup>1</sup>** (Fig. 1A) corresponds to the proton exchange between the Eu<sup>3+</sup>-bound water molecule and bulk solvent, whilst that at -11 ppm in the spectrum of **YbL<sup>1</sup>** (Fig. 1B and C) arises from the proton exchange between the amide proton and bulk water, based on analogy to previously reported DOTA-tetraamide complexes.<sup>19,32</sup> As expected, the temperature has a significant effect on the CEST spectra (Fig. S1 in Supplementary data), indicating an acceleration of the proton exchange at higher temperatures.

**EuL<sup>2</sup>** and **YbL<sup>2</sup>** show no CEST effect, either in the absence or in the presence of Ca<sup>2+</sup> (on addition of up to 20 equiv of Ca<sup>2+</sup>). In these

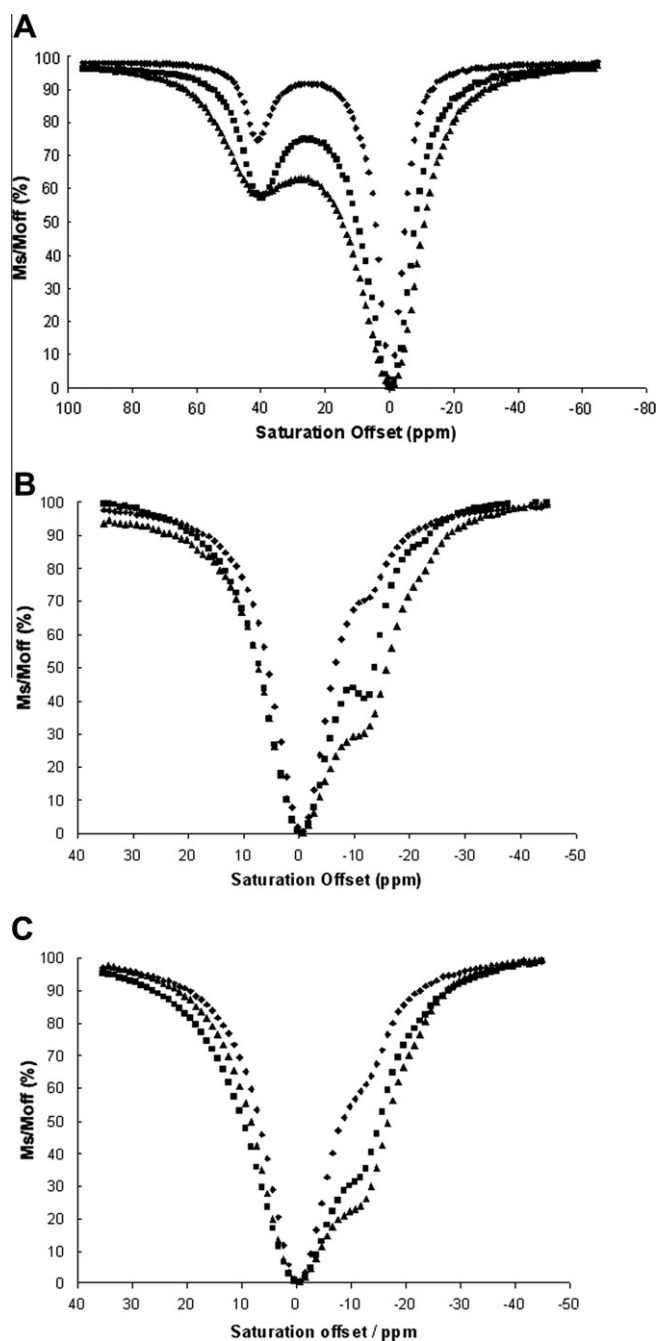


**Figure 1.** Solvent water signal intensity against presaturation frequency (CEST spectra). (A) Twenty millimolar aqueous solution of **EuL**<sup>1</sup> in the absence ( $\blacktriangle$ ) and in the presence of 5 ( $\blacksquare$ ) and 100 equiv ( $\blacklozenge$ ) of  $\text{Ca}^{2+}$ . (B) Twenty millimolar aqueous solution of **YbL**<sup>1</sup> in the absence ( $\blacktriangle$ ) and in the presence of 5 ( $\blacksquare$ ) and 100 equiv ( $\blacklozenge$ ) of  $\text{Ca}^{2+}$ . (C) Twenty millimolar aqueous solution of **YbL**<sup>1</sup> in the absence ( $\blacktriangle$ ) and in the presence of 5 ( $\blacksquare$ ) and 100 equiv ( $\blacklozenge$ ) of  $\text{Mg}^{2+}$ . Three hundred and ten Kelvin, irradiation time 3 s,  $B_1 = 25 \mu\text{T}$ .

complexes, the proton exchange rate on the amide protons or on the coordinated water is probably too fast, thus we cannot detect a CEST effect from the water coordinated to  $\text{Eu}^{3+}$  or from the amide proton in **YbL**<sup>2</sup>, as observed for the corresponding **L**<sup>1</sup> analogues. To the best of our knowledge, no bis(amide) complex of  $\text{Eu}^{3+}$  or  $\text{Yb}^{3+}$  has ever been reported to show a CEST effect. The water exchange rate has been previously determined on cyclen-*trans*-bis(amide)-bis(acetate) complexes of  $\text{Gd}^{3+}$ .<sup>33</sup> For the bis(dimethyl) amide analogue, the water exchange rate constants were found to be very different for the **m** and **M** isomers,  $7.0 \times 10^7 \text{ s}^{-1}$  and  $7.4 \times 10^5 \text{ s}^{-1}$ ,

respectively (the *m/M* ratio was  $\sim 0.7$  for the  $\text{Eu}^{3+}$  complex). These values are around two orders of magnitude higher than those reported for the tetraamide **EuDOTAM** complex with a known PARACEST effect, for instance ( $3.3 \times 10^5 \text{ s}^{-1}$  and  $8.3 \times 10^3 \text{ s}^{-1}$  for **m** and **M** isomers, respectively).<sup>34</sup> One should also note that the water exchange rate (as assessed by  $^{17}\text{O}$  NMR spectroscopy) and the proton exchange rate (assessed by  $^1\text{H}$  NMR) are identical for these types of complexes.<sup>33</sup> We have not determined the water exchange rate on **GdL**<sup>2</sup>, which should be close to the water (and proton) exchange on **EuL**<sup>2</sup>. However, we expect that it is in the same order of magnitude as the one reported for the  $\text{Gd}^{3+}$  bis(dimethyl) amide DOTA complex<sup>32</sup> which is clearly too fast and therefore prevents the observation of a CEST effect on **EuL**<sup>2</sup>.

It is more surprising that the **YbL**<sup>2</sup> complex does not show a CEST peak either, as the proton exchange on the two amide nitrogens would be expected to be slow, within the appropriate time-scale to produce CEST. It seems, however, that the presence of the neighbouring carboxylates contributes to a faster proton exchange. The amide protons are not visible in the high resolution  $^1\text{H}$  NMR spectrum (Supplementary data). Temperature variations within the range of 288–323 K had no effect on the recorded CEST spectra which only showed the direct saturation of water.

To investigate the sensitivity of  $\text{Eu}^{3+}$  and  $\text{Yb}^{3+}$  complexes of **L**<sup>1</sup> toward  $\text{Ca}^{2+}$  and  $\text{Mg}^{2+}$ , we have measured the CEST effect as a function of the  $\text{Ca}^{2+}$  and  $\text{Mg}^{2+}$  concentrations. Some representative CEST spectra are shown in Figure 1. In the absence of calcium ions, the complexes exhibited a CEST effect of 60% and 35% for **YbL**<sup>1</sup> and **EuL**<sup>1</sup>, respectively. Upon addition of calcium the CEST effect decreased sensibly for both chelates. In the case of **YbL**<sup>1</sup>, the decrease of the CEST effect is accompanied by a small shift of the amide proton resonance to  $\sim -13$  ppm (see also the high resolution  $^1\text{H}$  NMR spectra; Fig. S2 in Supplementary data). The addition of  $\text{Mg}^{2+}$  to the **YbL**<sup>1</sup> complex has a similar influence on the CEST effect observed (Fig. 1C).

By plotting the relative CEST magnitude ( $1 - M_s/M_0$ ) for the peak at  $-13$  ppm as a function of the  $[\text{Ca}]/[\text{YbL}^1]$  ratio, we obtain a curve that reaches saturation from a  $[\text{Ca}]/[\text{YbL}^1]$  ratio above  $\sim 40$  (Fig. 2; here  $M_s$  and  $M_0$  correspond to the water signal intensity at  $-13$  ppm (on resonance) and  $+13$  ppm (off resonance)). These data points have been fitted to estimate an affinity constant between **YbL**<sup>1</sup> and  $\text{Ca}^{2+}$ , by assuming that the observed overall CEST magnitude is the sum of contributions originating from the free **YbL**<sup>1</sup> and from the  $\text{Ca}^{2+}$ -bound **YbL**<sup>1</sup> species. We have assumed binding of a single  $\text{Ca}^{2+}$  cation per **YbL**<sup>1</sup> complex. The conditional affinity constant determined by this method is relatively low,  $K_{\text{aff}}^{\text{YbL}^1-\text{Ca}} = 8 \pm 2 \text{ M}^{-1}$ , at pH 7.4. For the complexation of  $\text{Ca}^{2+}$  with the iminodiacetate (IDA) ligand, the formation of 1:1 and 1:2

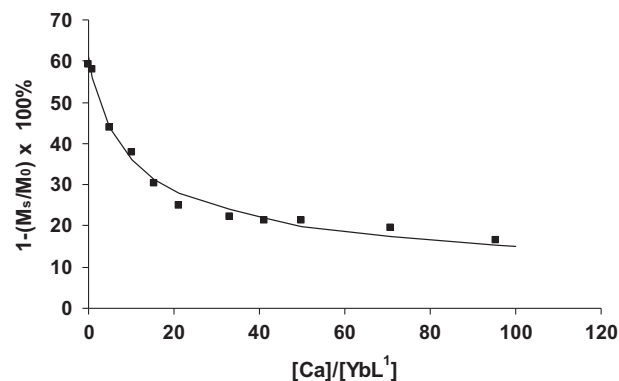


**Figure 2.** Variation of the CEST effect observed at  $-13$  ppm upon addition of  $\text{Ca}^{2+}$  to the **YbL**<sup>1</sup> complex.  $[\text{YbL}^1] = 0.02 \text{ M}$ , pH 7.4,  $T = 37^\circ\text{C}$ . The line represents the fit to the data points as explained in the text.

species have been described, with thermodynamic stability constants of  $\log K_1 = 3.3$  and  $\log K_2 = 2.7$ .<sup>35</sup> Taking into consideration of the protonation constants of IDA, for pH 7.4 we can calculate a conditional stability constant of  $\beta_{\text{cond}} = 1.3 \times 10^4 \text{ M}^{-1}$  or  $K_{\text{cond}} = 19 \text{ M}^{-1}$  assuming the formation of  $\text{Ca}(\text{IDA})_2$  or  $\text{Ca}(\text{IDA})$  species, respectively. The value obtained for the  $\text{YbL}^1\text{-Ca}^{2+}$  adduct,  $K_{\text{aff}}^{\text{YbL}^1\text{-Ca}} = 8 \text{ M}^{-1}$ , is close to the conditional stability constant calculated for the  $\text{Ca}^{2+}$  complex formed with one iminodiacetate unit. This suggests the binding of one iminodiacetate per  $\text{Ca}^{2+}$ . The coordination of a second IDA is likely to be hindered by steric constraints; all amide oxygens are coordinated to the lanthanide ion, and the ethylene linker between the amide nitrogen and the imino nitrogen is too short to provide enough flexibility so that a second IDA unit could turn towards the  $\text{Ca}^{2+}$  coordinated by a neighbouring pending arm.

We could also consider that the four IDA units are independent with respect to  $\text{Ca}^{2+}$  coordination and can each coordinate a cation. By analysing the data in this way, for the  $\text{YbL}^1\text{-Ca}$  system we obtain  $K_{\text{aff}}^{\text{YbL}^1\text{-Ca}} = 11 \pm 2$ , and the quality of the fit is as good as that in Figure 2. However, we believe that the coordination of four calcium ions is highly improbable due to steric reasons. The data can be also fitted by assuming the binding of two or three  $\text{Ca}^{2+}$  ions to one LnL chelate, with constants obtained between  $K_{\text{aff}}^{\text{YbL}^1\text{-Ca}} = 8$  and 11. We should note that, in either of the cases, the value of the affinity constant is close to the conditional constant for  $\text{Ca}(\text{IDA})$  (1:1 complex).

On the other hand, if there were more than one calcium ions coordinated to the LnL<sup>1</sup> complex, very likely the different sites of coordination could not be considered as independent, but a successive binding model should be rather used. Unfortunately, all attempts to try to fit more than one constant were unsuccessful. It could be reasonable to include also the  $\text{Ca}(\text{IDA})_2$  species. However,

we could never obtain a reasonable value for the formation of 1:2 species. Therefore we decided to fit the data with the simplest model that gives a good quality fit.

The interaction between  $\text{YbL}^1$  and  $\text{Mg}^{2+}$  has been also evaluated in a similar manner to yield  $K_{\text{aff}}^{\text{YbL}^1\text{-Mg}} = 23 \pm 3 \text{ M}^{-1}$  (Fig. S3 in Supplementary data). The affinity constant is slightly higher than that obtained for the  $\text{YbL}^1\text{-Ca}$  interaction. This is in good agreement with the higher stability constant reported for the  $\text{Mg}(\text{IDA})$  complex ( $\log K_1 = 3.66$ )<sup>36</sup> compared to the  $\text{Ca}^{2+}$  analogue. Given the smaller size of  $\text{Mg}^{2+}$ , the coordination of a second iminodiacetate unit is even less probable. Indeed, no 1:2 complex has been detected in the  $\text{Mg}^{2+}\text{-IDA}$  system either.<sup>35</sup> In the case of  $\text{EuL}^1$ , the variation of the CEST magnitude at 26 ppm has been plotted as a function of the  $[\text{Ca}]/[\text{EuL}^1]$  ratio, and fitted analogously to  $\text{YbL}^1$ . The affinity constant determined for the  $\text{EuL}^1\text{-Ca}^{2+}$  interaction is  $K_{\text{aff}}^{\text{EuL}^1\text{-Ca}} = 10 \pm 3 \text{ M}^{-1}$ , in good agreement with the value for  $\text{YbL}^1$  (Fig. S4 in Supplementary data). We should note that due to the smaller variation of the CEST effect, the estimation of  $K_{\text{aff}}$  is less precise than in the case of  $\text{YbL}^1$ .

When responsive agents are developed for MRI detection, the selectivity towards to the cation (or other species) is an important requirement. Our system does not show any selectivity for  $\text{Ca}^{2+}$  over the chemically similar and biologically available  $\text{Mg}^{2+}$ . The concentration of free  $\text{Ca}^{2+}$  is slightly higher in the extracellular medium, 1.0 mM with respect to 0.7 mM for  $\text{Mg}^{2+}$  in the cerebrospinal fluid.<sup>9</sup> In the plasma, the difference is more significant: 1.4 mM for free  $\text{Ca}^{2+}$  and 0.5 mM for free  $\text{Mg}^{2+}$ . However, given the predominance in number of  $\text{Ca}^{2+}$  channels and transporters,<sup>37</sup> the variation in the  $\text{Mg}^{2+}$  concentration in comparison to variation in the  $\text{Ca}^{2+}$  concentration during the neural activity should be minimal. Thus changes in  $\text{Ca}^{2+}$  concentration are more likely dominate over the changes in  $\text{Mg}^{2+}$  concentration. We should also note that

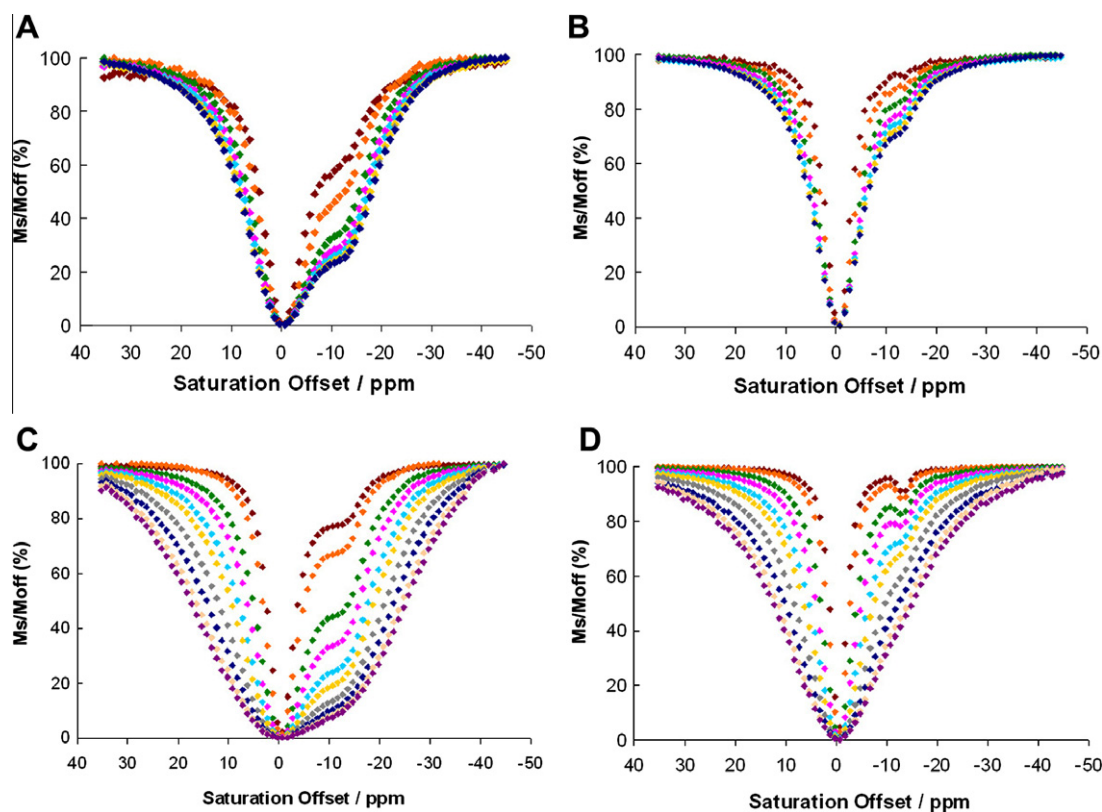


**Fig. 3.** CEST spectra of  $\text{YbL}^1$  recorded with variable irradiation times in the absence (A) and in the presence of 100 equiv of calcium (B). Irradiation times from top to bottom: 0.25, 0.5, 1, 1.5, 2, 3, 4, 5 s. CEST spectra of  $\text{YbL}^1$  recorded with variable saturation power in the absence (C) and in the presence of 100 equiv of calcium (D). Saturation power from top to bottom: 36, 34, 30, 28, 26, 24, 22, 20, 18 and 17 dB.  $T = 37^\circ \text{C}$ .

Zn<sup>2+</sup> or Cu<sup>2+</sup> (which are the most abundant divalent endogenous cations after Ca<sup>2+</sup> and Mg<sup>2+</sup>) are much less concentrated (micromolar range) and should not interfere in the detection of Ca<sup>2+</sup>. These factors can contribute to a reliable detection of calcium with **L**<sup>1</sup> despite the low selectivity.

The CEST effect is directly related to the rate of the proton exchange between the bulk solvent and the amide (for **YbL**<sup>1</sup>) or the coordinated water site (for **EuL**<sup>1</sup>). The exchange rate can be quantitatively assessed from the saturation time and saturation power dependency of the water proton intensity.<sup>38</sup> We performed QUEST and QUESP experiments (quantification of the exchange rate as a function of saturation time or saturation power, respectively), to determine the exchange rate for the **YbL**<sup>1</sup> system in the absence and in the presence of Ca<sup>2+</sup> or Mg<sup>2+</sup>.

Figure 3 shows the effect of saturation power and irradiation time on the transfer of saturation from the amide proton to the bulk water pool for **YbL**<sup>1</sup> in the absence and in the presence of 100 equiv of Ca<sup>2+</sup>. Analogous data have been recorded in the presence of 100 equiv of Mg<sup>2+</sup> (shown in the Supplementary data). The **YbL**<sup>1</sup> complex has been chosen for these experiments since the effect of the alkaline earth cations is more important than with **EuL**<sup>1</sup>. The results (Fig. 3A and B) indicate that the CEST effect does not increase when the saturation time is increased beyond 2 s. On the other hand, we observe that a high pulse power produces a large increase of the CEST effect (Fig. 3C and D).

Figure 4A and B show the dependence of the CEST effect (measured at –13 ppm) on the saturation time and on the saturation power in the absence and in the presence of calcium, respectively. The data have been fitted to Eqs. 2–5 to obtain the rate of proton exchange.

Assuming that the steady state is reached upon saturation of the solute, the following equation applies for the measured CEST effect,<sup>37</sup>

$$1 - \frac{M_s}{M_0} = \frac{k_{\text{ex}} \cdot \alpha \cdot x_{\text{CA}}}{R_{1W} + k_{\text{ex}} \cdot x_{\text{CA}}} \times [1 - e^{-(R_{1W} + k_{\text{ex}} \cdot x_{\text{CA}})t_{\text{sat}}}] \quad (2)$$

where  $x_{\text{CA}}$  is the fractional concentration of the exchangeable protons of the contrast agent,  $t_{\text{sat}}$  is the saturation time,  $\alpha$  is the saturation efficiency, and  $k_{\text{ex}}$  is the rate of proton exchange on the amide. The saturation efficiency depends on the pulse power via the following equation:

$$\alpha = \frac{\omega_1^2}{\omega_1^2 + p \cdot q} \quad (3)$$

where

$$p = R_{2S} + k_{\text{ex}} - \frac{k_{\text{ex}}^2 \cdot x_{\text{CA}}}{R_{2W} + k_{\text{ex}} \cdot x_{\text{CA}}} \quad (4)$$

$$q = R_{1S} + k_{\text{ex}} - \frac{k_{\text{ex}}^2 \cdot x_{\text{CA}}}{R_{1W} + k_{\text{ex}} \cdot x_{\text{CA}}} \quad (5)$$

where  $R_{1,2S}$  and  $R_{1,2W}$  are the longitudinal and transverse relaxation rates during saturation of the solute and of the bulk water, respectively. The expression given in Eq. 2 reaches the same maximum CEST effect as predicted by Sherry et al.<sup>18</sup> and Aime et al.<sup>39</sup> assuming complete saturation.

We have made the assumption that  $R_{1W}$  and  $R_{2W}$  can be approximated by the relaxation rates measured for bulk water<sup>32</sup> in a solution containing 20 mM **YbL**<sup>1</sup> (with or without Ca<sup>2+</sup>/Mg<sup>2+</sup>). These values have been therefore determined by independent measurements using inversion recovery and Carr–Purcell–Meiboom–Gill sequences and were fixed during the fit (Table 1). The longitudinal and transverse relaxation rates of the solute  $R_{1,2S}$  (in Eqs. 4 and 5) have been calculated in the fit. We should note that  $R_{1S}$  is negligible as compared to  $k_{\text{ex}}$  and has no influence on the fit. Table 1 demonstrates that the presence of Ca<sup>2+</sup> or Mg<sup>2+</sup> salts have essentially no effect on any of the relaxation rates. The best fitting values for  $k_{\text{ex}}$  and the relaxation rates determined independently are listed in Table 1.

We should note that we have also analysed the  $1 - M_s/M_0$  values obtained as a function of the saturation time for all three systems (**YbL**<sup>1</sup> without and with Ca<sup>2+</sup>/Mg<sup>2+</sup>) according to Eq. 6, as reported by Zhang et al.<sup>17</sup> Here we have fitted both  $k_{\text{ex}}$  and  $R_{1W}$  and obtained very similar values for the exchange rate (within 10%) as in the simultaneous fit of the saturation time dependent and saturation power dependent CEST data to Eq. 2.

$$1 - \frac{M_s}{M_0} = 1 - \left( \frac{R_{1W}}{R_{1W} + k_{\text{ex}} \cdot x_{\text{CA}}} + \frac{k_{\text{ex}} \cdot x_{\text{CA}}}{R_{1W} + k_{\text{ex}} \cdot x_{\text{CA}}} e^{-(R_{1W} + k_{\text{ex}} \cdot x_{\text{CA}})t_{\text{sat}}} \right) \quad (6)$$

The exchange rate of the amide proton obtained for **YbL**<sup>1</sup> is in good agreement with those reported in the literature for tetraamide DOTA-derivative Yb<sup>3+</sup> complexes. For instance,  $k_{\text{ex}} = 1724 \text{ s}^{-1}$

**Table 1**

$k_{\text{ex}}$  values calculated from the best fit of QUEST and QUESP data and relaxation rates obtained in the fit or determined in independent inversion recovery ( $R_{1W}$ ) or CPMG ( $R_{2W}$ ) experiments

|                                    | <b>YbL</b> <sup>1</sup> | <b>YbL</b> <sup>1</sup> + 100 equiv Ca <sup>2+</sup> | <b>YbL</b> <sup>1</sup> + 100 equiv Mg <sup>2+</sup> |
|------------------------------------|-------------------------|--|--|
| $k_{\text{ex}}$ (s <sup>-1</sup> ) | 2100 ± 150              | 210 ± 20   | 309 ± 20   |
| $R_{1S}$ (s <sup>-1</sup> )        | 0.624                   | 0.624  | 0.624  |
| $R_{2S}$ (s <sup>-1</sup> )        | 588                     | 588  | 588  |
| $R_{1W}$ (s <sup>-1</sup> )        | 0.269                   | 0.262  | 0.262  |
| $R_{2W}$ (s <sup>-1</sup> )        | 0.271                   | 0.263  | 0.263  |
| $x_{\text{CA}}$                    | 0.00072                 | 0.0006   | 0.0006   |

Three hundred and ten Kelvin, pH 7.4.

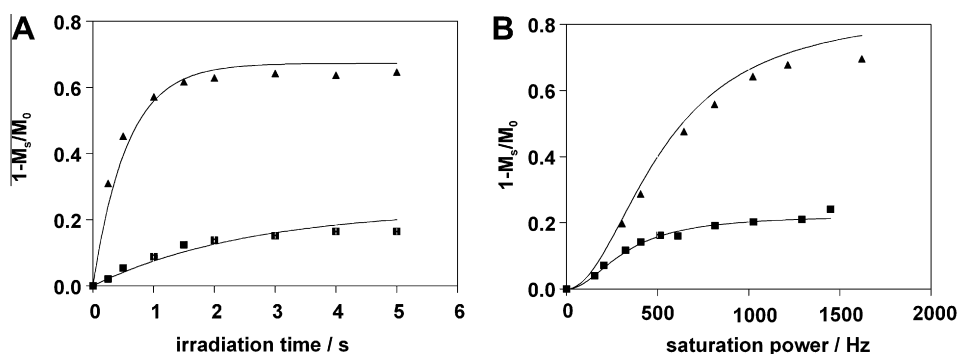


**Fig. 4.** QUEST and QUESP results with best fits to the Eqs. 2–5. (A) Plot of the magnetisation as a function of the saturation time for **YbL**<sup>1</sup> in the absence ( $\blacktriangle$ ) and in the presence of 100 equiv of calcium ( $\blacksquare$ ). (B) Plot of the magnetisation as a function of the saturation power for **YbL**<sup>1</sup> in the absence ( $\blacktriangle$ ) and in the presence of 100 equiv of calcium ( $\blacksquare$ ). The curves represent the fit as explained in the text.

was determined for YbDOTAM (at 298 K and pH 7.4),<sup>39</sup>  $k_{\text{ex}} = 2500 \text{ s}^{-1}$  for the glycinate derivative YbDOTAMGly (at 312 K and pH 8.1),<sup>40</sup> or  $k_{\text{ex}} = 1111 \text{ s}^{-1}$  for the tetra(glycine-phenylalanine) derivative YbDOTAMGly-Phe (at 311 K, pH 7.0).<sup>27</sup> Upon addition of  $\text{Ca}^{2+}$  or  $\text{Mg}^{2+}$  to the **YbL**<sup>1</sup> complex, the exchange rate of the amide proton decreases significantly which is then translated as a diminution of the observed CEST effect. If we assume that there is one alkaline earth cation bound per **YbL**<sup>1</sup> chelate and it is bound to a single iminodiacetate arm as suggested by the affinity constant (vide infra), the amide protons become non-equivalent and the reported exchange rate is an effective (average) value. A diminution of the amide proton exchange rate has been previously reported for the tetraglycinate derivative LnDOTAMGly complexes when decreasing the pH from 8.1 to 6.0 (e.g.,  $k_{\text{ex}} = 2500 \text{ s}^{-1}$  at pH 8.1 for YbDOTAMGly in comparison to  $k_{\text{ex}} = 125\text{--}128 \text{ s}^{-1}$  for Ln = Eu, Nd, Pr at pH 6,  $T = 312 \text{ K}$ ).<sup>40</sup> The slower proton exchange resulted in a subsequent diminution or disappearance of the observed CEST effect, similar to what we observe upon addition of the alkaline earth metal ions to **YbL**<sup>1</sup>. One possible explanation of the slower amide proton exchange on the  $\text{Ca}^{2+}$ -bound species can be related to a change in the protonation state of the iminodiacetate group. In the absence of  $\text{Ca}^{2+}$ , the nitrogen of the iminodiacetate moiety is protonated at pH 7.4, and the presence of this proton on the amine can contribute to a faster exchange ( $\log K_{\text{H}} = 9.32$  for the nitrogen of IDA, while a lower value,  $\log K_{\text{H}} = 8.17$  was reported for the *N*-acetyl-1,2-diaminoethane-*N',N'*-diacetic acid that has a structure similar to the pending arm of **L**<sup>1</sup>).<sup>41</sup> Upon  $\text{Ca}^{2+}$  coordination, the amine is deprotonated and this catalytic effect is no longer operating. On the other hand, the charge of the iminodiacetate unit also changes on  $\text{Ca}^{2+}$  coordination from  $-1$  to  $0$  which could also influence the proton exchange on the neighbouring amide.

Although in PARACEST imaging the role of the contrast agent concentration might be considered less critical as compared to  $\text{Gd}^{3+}$ -based agents (the CEST effect becomes independent of concentration after a certain limit), a precise knowledge of the local concentration of the agent can be still important for an accurate determination of the cation to be sensed in real applications. In order to circumvent the problem of not knowing the local concentration of the agent, ratiometric methods have been proposed either by using a probe endowed with multiple exchange sites (coordinated water and amide protons) that have a different response to the analyte or by applying two distinct molecules (two different lanthanide complexes) with a different CEST response. This second approach can be realised when a mixture of **YbL**<sup>1</sup> and **EuL**<sup>1</sup> is used

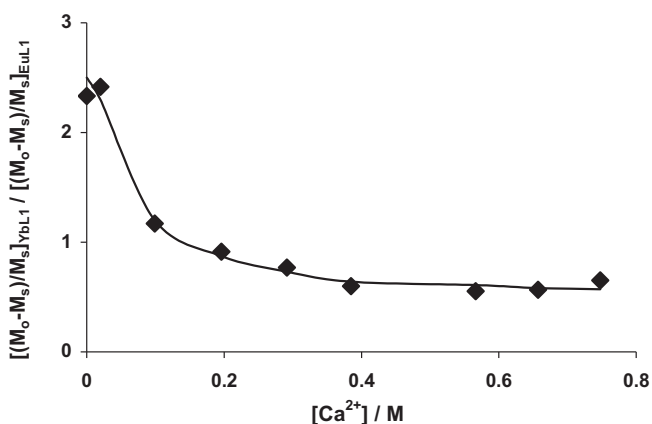


**Fig. 5.** Calcium dependence of the relative CEST effect (independent of the **LnL**<sup>1</sup> complex concentration) as resulting from the ratiometric method by simultaneously using **EuL**<sup>1</sup> and **YbL**<sup>1</sup>.  $c_{\text{EuL}^1} = c_{\text{YbL}^1} = 20 \text{ mM}$ ; 310 K, irradiation time 3 s,  $B_1 = 25 \mu\text{T}$ . (The line was drawn to guide the eyes.)

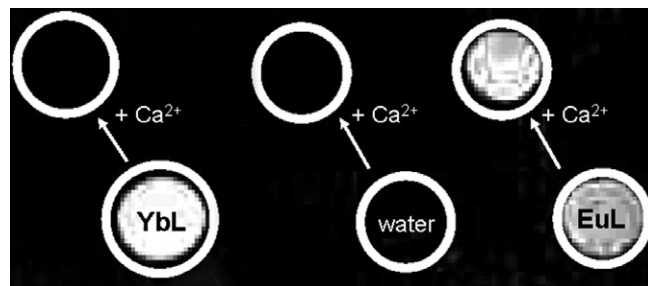


**Fig. 6.** CEST images of phantoms containing water or a solution of 20 mM **YbL**<sup>1</sup> and **EuL**<sup>1</sup> before (bottom) and after (top) addition of calcium. The CEST images represent the intensity difference between the spin-echo images for saturation at  $\delta = -11 \text{ ppm}$  and  $\delta = +11 \text{ ppm}$  (**YbL**<sup>1</sup>) or at  $\delta = +41 \text{ ppm}$  and  $\delta = +26 \text{ ppm}$  (**EuL**<sup>1</sup>), 23 °C.

which provides differing CEST responses to  $\text{Ca}^{2+}$ . For the two analogous complexes, one can expect identical biodistribution, therefore the ratio of the CEST effect detected at  $-13 \text{ ppm}$  (for **YbL**<sup>1</sup>) and  $+41 \text{ ppm}$  (**EuL**<sup>1</sup>) will be independent of the absolute concentration of the complexes. This ratio has been plotted as a function of the  $\text{Ca}^{2+}$  concentration (Fig. 5). Up to  $0.5 \text{ M}$   $\text{Ca}^{2+}$ , this ratio changes considerably, whilst at higher concentrations it becomes constant.

To demonstrate that  $\text{Ca}^{2+}$  binding can be sensed in a CEST imaging experiment, a phantom consisting of plastic tubes, each containing 20 mM **EuL**<sup>1</sup> or **YbL**<sup>1</sup> in presence or absence of  $\text{Ca}^{2+}$  ions, was prepared. Images were acquired after applying a selective 3 s presaturation pulse at  $\delta = 41 \text{ ppm}$  and  $\delta = -11 \text{ ppm}$  for **EuL**<sup>1</sup> and **YbL**<sup>1</sup>, respectively. A second image was collected after presaturation at  $\delta = 26 \text{ ppm}$  and  $\delta = 11 \text{ ppm}$  and CEST images were generated through pixel-by-pixel subtraction of the two images. The intensities of the CEST images (Fig. 6) show a clear difference after addition of calcium ions.

### 3. Conclusions

We have described the synthesis and evaluation of a new family of calcium-activated PARACEST contrast agents. The sensors that combine a  $\text{Ln}^{3+}$  chelating unit with an aminocarboxylate-based moiety for calcium binding resulting in marked variations in the CEST effect in response to  $\text{Ca}^{2+}$ . The affinity constants between the lanthanide complexes and the alkaline earth metal ions have been estimated from the variation of the CEST effect to be  $K_{\text{aff}}^{\text{YbL}^1-\text{Ca}} = 8 \pm 2 \text{ M}^{-1}$ ,  $K_{\text{aff}}^{\text{YbL}^1-\text{Mg}} = 23 \pm 3 \text{ M}^{-1}$  and  $K_{\text{aff}}^{\text{EuL}^1-\text{Ca}} = 10 \pm 3 \text{ M}^{-1}$ . These low values suggest the coordination of the alkaline earth ions to a single iminodiacetate arm.  $\text{Ca}^{2+}/\text{Mg}^{2+}$  binding to the lanthanide complexes slows down the exchange of the amide protons on **YbL**<sup>1</sup> which is responsible for the diminished CEST effect. **EuL**<sup>1</sup> and **YbL**<sup>1</sup> are able to produce a variation of the MRI signal along with the change of calcium concentration.

### 4. Experimental

#### 4.1. General procedures

<sup>1</sup>H NMR and <sup>13</sup>C{<sup>1</sup>H} NMR spectra were recorded on Bruker Avance II 300 MHz 'Microbay' spectrometer at room temperature. ESI-HRMS were performed on a Bruker BioApex II ESI-FT-ICR, equipped with an Agilent ESI-Source, measured via flow injection analysis. ESI-LRMS were performed on a ion trap SL 1100 system (Agilent, Germany). Column chromatography was performed using silicagel 60 (70–230 mesh ASTM) from Merck, Germany. DO2AtBu (4) was purchased from CheMatech, Dijon, France.

## 4.2. Synthesis of the ligand

### 4.2.1. Compound 2

Cyclen (59 mg, 0.34 mmol) was dissolved in CH<sub>3</sub>CN (10 ml), K<sub>2</sub>CO<sub>3</sub> (458 mg, 3.31 mmol) was added and the suspension was stirred for 15 min. Bromide **1** (465 mg, 1.65 mmol) in CH<sub>3</sub>CN (10 ml) was added dropwise and the mixture was heated at 80 °C for 18 h. After cooling the solid material was removed by filtration, the solvent was evaporated and the residue purified by column chromatography (CH<sub>2</sub>Cl<sub>2</sub>/CH<sub>3</sub>OH 92:8) to yield 290 mg (88%) of **2**. Analytical data match to those previously reported for this molecule.<sup>30</sup>

### 4.2.2. *tert*-Butoxycarbonylmethyl-2-[2-(4,7,10-tris-[[2-(bis-*tert*-butoxycarbonylmethyl-amino)-ethylcarbamoyl]-methyl]-1,4,7,10tetraaza-cyclododec-1-yl)-acetyl-amino]-ethyl)-amino-acetic acid *tert*-butyl ester (**3**)

Protected amine **2** (660 mg, 0.68 mmol), was dissolved in 1.25 M methanolic HCl (20 ml) and the solution was stirred at room temperature for 18 h. The solvent was removed on the rotary evaporator and the residue was dissolved in water (5 ml). The pH of the solution was adjusted to neutral using 5 M NaOH and the water was removed on the rotary evaporator. The solid residue and K<sub>2</sub>CO<sub>3</sub> (1.87 g, 13.53 mmol) were suspended in CH<sub>3</sub>CN (20 ml) and the mixture was stirred for 30 min. *tert*-Butyl bromoacetate (1.32 g, 6.77 mmol) in CH<sub>3</sub>CN (10 ml) was finally added dropwise and the mixture was heated at 80 °C for 18 h. After cooling the suspension was filtered, the solvent was evaporated and the residue purified by column chromatography (CH<sub>2</sub>Cl<sub>2</sub>/CH<sub>3</sub>OH 96:4) to yield 533 mg (53%) of **3** as yellow viscous oil which solidifies upon standing.

<sup>1</sup>H NMR (CDCl<sub>3</sub>, 300 MHz): δ = 7.63 (br s, 4H), 3.34 (s, 16H), 3.24–3.14 (br, 8H), 3.12–3.03 (br, 8H), 2.80–2.70 (br, 8H), 2.67–2.48 (br, 8H), 2.43–2.27 (br, 8H), 1.38 (s, 72H). <sup>13</sup>C{<sup>1</sup>H} NMR (CDCl<sub>3</sub>, 75 MHz): δ = 171.1, 170.8, 81.2, 57.1, 55.8, 52.7, 50.4, 37.3, 28.0. ESI-HRMS: for C<sub>72</sub>H<sub>133</sub>N<sub>12</sub>O<sub>20</sub><sup>+</sup>: calcd 1485.9754 [M+H]<sup>+</sup>, found 1485.9847; for C<sub>72</sub>H<sub>132</sub>N<sub>12</sub>NaO<sub>20</sub><sup>+</sup>: calcd 1507.9573 [M+Na]<sup>+</sup>, found 1507.9577.

### 4.2.3. (Carboxymethyl-2-[2-(4,7,10-tris-[[2-(bis-carboxymethyl-amino)-ethylcarbamoyl]-methyl]-1,4,7,10tetraaza-cyclododec-1-yl)-acetyl-amino]-ethyl)-amino)-acetic acid (**L**<sup>1</sup>)

Compound **3** (128 mg, 0.086 mmol) was dissolved in formic acid (5 ml) and the solution was heated at 60 °C for 18 h. After the solution was cooled, formic acid was removed on the rotary evaporator. The residue was dissolved in minimal amount of water, added dropwise to cooled acetone (–20 °C) and stored in the freezer overnight. The acetone was decanted from the solid material and the crude product was obtained by drying it under reduced pressure to afford 73 mg (82%) of **L**<sup>1</sup> as colourless hygroscopic solid.

<sup>1</sup>H NMR (D<sub>2</sub>O, 300 MHz): δ = 3.91–3.79 (br, 24H), 3.61–3.52 (br, 8H), 3.39–3.32 (br, 8H), 3.31–3.18 (br, 16H). <sup>13</sup>C{<sup>1</sup>H} NMR (D<sub>2</sub>O, 75 MHz): δ = 169.6, 56.6, 55.6, 54.3, 50.0, 34.7. ESI-HRMS: for C<sub>40</sub>H<sub>67</sub>N<sub>12</sub>O<sub>20</sub><sup>-</sup>: calcd 1035.4600 [M–H]<sup>-</sup>, found 1035.4633; for C<sub>40</sub>H<sub>66</sub>N<sub>12</sub>O<sub>20</sub><sup>2-</sup>: calcd 517.2264 [M–2H]<sup>2-</sup>, found 517.2259.

### 4.2.4. {4,10-Bis-[[2-(benzyloxycarbonylamino)-ethylcarbamoyl]-methyl]-7-*tert*-butoxycarbonylmethyl-1,4,7,10tetraaza-cyclododec-1-yl]-acetic acid *tert*-butyl ester, **6**

DO2AtBu (**4**, 467 mg, 1.17 mmol) was dissolved in dry DMF (3 ml) and K<sub>2</sub>CO<sub>3</sub> (776 mg, 5.61 mmol) was added. After stirring for 30 min, benzyl 2-(2-bromoacetamido)ethylcarbamate (**5**, 882 mg, 2.80 mmol) in DMF (2 ml) was added slowly and suspension was stirred for 24 h at room temperature. After that period the suspension was filtered, the solvent was evaporated and the resi-

due was purified by column chromatography (CH<sub>2</sub>Cl<sub>2</sub>/CH<sub>3</sub>OH 93:7) to afford 764 mg (75%) of **6** as yellow viscous oil which solidifies upon standing.

<sup>1</sup>H NMR (CDCl<sub>3</sub>, 300 MHz): δ = 7.79 (br s, 2H), 7.29–7.16 (m, 10H), 6.06 (br s, 2H), 4.99 (s, 4H), 3.33–3.08 (br, 12H), 3.02–2.75 (br, 4H), 2.55–1.95 (br, 16H), 1.32 (s, 18H). <sup>13</sup>C{<sup>1</sup>H} NMR (CDCl<sub>3</sub>, 75 MHz): δ = 172.1, 171.7, 156.8, 136.9, 128.3, 127.8, 127.7, 81.6, 66.2, 56.2, 55.5, 50.4, 40.9, 39.6, 28.0. ESI-HRMS: for C<sub>44</sub>H<sub>69</sub>N<sub>8</sub>O<sub>10</sub><sup>+</sup>: calcd 869.5131 [M+H]<sup>+</sup>, found 869.5165; for C<sub>44</sub>H<sub>68</sub>N<sub>8</sub>NaO<sub>10</sub><sup>+</sup>: calcd 891.4951 [M+Na]<sup>+</sup>, found 891.4953.

### 4.2.5. {4,10-Bis-[[2-(2-amino-ethylcarbamoyl)-methyl]-7-*tert*-butoxycarbonylmethyl-1,4,7,10tetraaza-cyclododec-1-yl]-acetic acid *tert*-butyl ester, **7**

Compound **6** (764 mg, 0.88 mmol) was dissolved in CH<sub>3</sub>OH (50 ml) and Pd/C (200 mg) was added. After the hydrogenation at 2.5 bar (18 h), suspension was filtered through celite and solvent was evaporated to give **7** containing carbamate residues.

<sup>1</sup>H NMR (CDCl<sub>3</sub>, 300 MHz): δ = 7.98 (br s, 2H), 3.32–3.17 (br, 8H), 3.13–2.89 (br, 8H), 2.84–2.73 (br, 4H), 2.64–2.13 (br, 16H), 1.37 (s, 18H). <sup>13</sup>C{<sup>1</sup>H} NMR (CDCl<sub>3</sub>, 75 MHz): δ = 171.9, 171.6, 81.5, 56.3, 55.5, 50.5, 50.1, 41.6, 41.3, 28.0. ESI-HRMS: for C<sub>28</sub>H<sub>56</sub>N<sub>8</sub>NaO<sub>6</sub><sup>+</sup>: calcd 623.4215 [M+Na]<sup>+</sup>, found 623.4223.

### 4.2.6. (4,10-Bis-[[2-(bis-*tert*-butoxycarbonylmethyl-amino)-ethylcarbamoyl]-methyl]-7-*tert*-butoxycarbonylmethyl-1,4,7,10tetraaza-cyclododec-1-yl)-acetic acid *tert*-butyl ester, **8**

Amine **7** (106 mg, 0.18 mmol), *tert*-butyl bromoacetate (172 mg, 0.88 mmol) and K<sub>2</sub>CO<sub>3</sub> (243 mg, 1.76 mmol) were mixed in CH<sub>3</sub>CN (10 ml) and the mixture was heated at 80 °C for 18 h. After cooling the suspension was filtered, the solvent was evaporated and the residue purified by column chromatography (CH<sub>2</sub>Cl<sub>2</sub>/CH<sub>3</sub>OH 97:3) to yield 99 mg (53%) of **8** as yellow viscous oil.

<sup>1</sup>H NMR (CDCl<sub>3</sub>, 300 MHz): δ = 7.61–7.56 (br, 2H), 3.34 (s, 8H), 3.22–3.10 (br, 8H), 3.06–2.92 (br, 4H), 2.79–2.72 (br, 4H), 2.69–2.42 (br, 8H), 2.40–2.19 (br, 8H), 1.39 (s, 36H), 1.37 (s, 18H). <sup>13</sup>C{<sup>1</sup>H} NMR (CDCl<sub>3</sub>, 75 MHz): δ = 171.7, 171.1, 171.0, 81.3, 56.5, 55.9, 55.6, 53.0, 50.6, 37.2, 28.1. ESI-HRMS: for C<sub>52</sub>H<sub>97</sub>N<sub>8</sub>O<sub>14</sub><sup>+</sup>: calcd 1057.7119 [M+H]<sup>+</sup>, found 1057.7139; for C<sub>52</sub>H<sub>96</sub>N<sub>8</sub>NaO<sub>14</sub><sup>+</sup>: calcd 1079.6938 [M+Na]<sup>+</sup>, found 1079.6926.

### 4.2.7. (4,10-Bis-[[2-(bis-carboxymethyl-amino)-ethylcarbamoyl]-methyl]-7-carboxymethyl-1,4,7,10tetraaza-cyclododec-1-yl)-acetic acid, **L**<sup>2</sup>

Compound **8** (269 mg, 0.254 mmol) was dissolved in formic acid (5 ml) and the solution was heated at 60 °C for 18 h. After the solution was cooled, formic acid was removed on the rotary evaporator. The residue was dissolved in minimal amount of water, added dropwise to cooled acetone (–20 °C) and stored in the freezer overnight. The acetone was decanted from the solid material and the crude product was obtained by its drying in the vacuum to afford 145 mg (79%) of **L**<sup>2</sup> as colourless hygroscopic solid.

<sup>1</sup>H NMR (D<sub>2</sub>O, 300 MHz): δ = 3.90–3.79 (br, 12H), 3.63–3.45 (br, 8H), 3.44–3.28 (br, 12H), 3.20–2.94 (br, 8H). <sup>13</sup>C{<sup>1</sup>H} NMR (D<sub>2</sub>O, 75 MHz): δ = 169.7, 56.5, 55.5, 54.8, 51.1, 48.6, 34.9. ESI-HRMS: for C<sub>28</sub>H<sub>47</sub>N<sub>8</sub>O<sub>14</sub><sup>+</sup>: calcd 719.3217 [M–H]<sup>-</sup>, found 719.3225.

### 4.2.8. Ln<sup>3+</sup> complexes

The Ln<sup>3+</sup> complexes of **L**<sup>1</sup> and **L**<sup>2</sup> were prepared by mixing the ligand and the LnCl<sub>3</sub> solutions in 1:1 ratio. The solution was stirred at 60 °C for 48 h and at room temperature for 24 h. The pH was adjusted to 7.0–7.5 using a solution of NaOH (1 M). After 72 h, the mixture was stirred for 24 h at room temperature in presence of Chelex 100. The absence of free Ln<sup>3+</sup> (Yb<sup>3+</sup> or Eu<sup>3+</sup>) was verified by colorimetric assay using xylenol orange.

#### 4.2.9. NMR measurements

All CEST experiments were carried out on Bruker Avance 500 MHz spectrometer. The saturation transfer experiments were carried out at 310 K by irradiating the sample at increments of 0.1 ppm. CEST spectra were recorded using pre-saturation pulses of 3 s duration at 20 and 25  $\mu$ T. Spectra were measured by recording the bulk water signal intensity as a function of the presaturation frequency.

For the QUEST experiments (quantification of the exchange rate as a function of saturation time), data was collected by varying the saturation time and keeping the power constant (25  $\mu$ T). The saturation times were 0.25, 0.5, 1, 1.5, 2, 3, 4, 5 s. QUESP data (quantification of the exchange rate as a function of saturation power) was collected by varying the saturation power whilst the saturation time remained constant (3 s). The saturation field strengths varied between 150 and 1620 Hz. The QUEST and QUESP data were both fit analytically with Scientist<sup>®</sup> (MicroMath<sup>®</sup>, Inc.).

The CaCl<sub>2</sub> and MgCl<sub>2</sub> solutions were made from the respective chloride salts in distilled water. The affinity constants were determined by adding CaCl<sub>2</sub> and MgCl<sub>2</sub> solutions to the LnL<sup>1</sup> solutions at pH 7.4 and recording the CEST effect at –13 ppm and +13 ppm for YbL<sup>1</sup> and at +42 ppm and –42 ppm for EuL<sup>1</sup>. The titrations were carried out at 37 °C.

#### 4.2.10. MRI measurements

Imaging experiments at a field strength of 16.4 T (corresponding to a proton Larmor frequency of 700 MHz) were performed on a Magnex magnet interfaced to a Bruker console. The samples were immersed in water to avoid susceptibility artefacts and heated to 37 °C throughout the experiments. Images were acquired using a RARE (rapid acquisition with relaxation enhancement) sequence, preceded by a 3 s magnetisation transfer pulse with a strength of 20  $\mu$ T. A repetition time of 7500 ms and four echoes were acquired per repetition, an inplane spatial resolution of 234  $\mu$ m with a slice thickness of 1 mm was obtained within 3 min. The data was reconstructed and difference images were formed using home-written Matlab (The MathWorks Inc., Natick, MA) routines.

#### Acknowledgements

The authors like to thank Dr. I. Mamedov for helpful discussions. Financial support from the DFG (Grant AN 716/2-1), Max-Planck Society, and the Centre National de la Recherche Scientifique (France) is gratefully acknowledged. This work was performed within the European COST Action D38.

#### Supplementary data

Supplementary data associated with this article can be found, in the online version, at doi:10.1016/j.bmc.2010.07.023.

#### References and notes

- Forsen, S.; Kordel, J. Calcium in Biological Systems. In *Bioinorganic Chemistry*; Bertini, I., Gray, H. B., Lippard, S. J., Valentine, J. S., Eds.; University Science Books: Mill Valley, CA, 1994; p 107.
- Tsien, R. Y. *Chem. Eng. News* **1994**, 72, 34.
- Tsien, R. W.; Tsien, R. Y. *Annu. Rev. Cell Biol.* **1990**, 6, 715.
- Meldolesi, J. *Nature* **1998**, 392, 863.
- Burgoyne, R. D. *Nat. Rev. Neurosci.* **2007**, 8, 182.
- Logothetis, N. K. *Nature* **2008**, 453, 869.
- Li, W.-H.; Fraser, S. E.; Meade, T. J. *J. Am. Chem. Soc.* **1999**, 121, 1413.
- Atanasijevic, T.; Shusteff, M.; Fam, P.; Jasanoff, A. *Proc. Natl. Acad. Sci. U.S.A.* **2006**, 103, 14707.
- Somjen, G. G. *Ions in the Brain: Normal Function, SEIZURES, and Stroke*; Oxford University Press: New York, 2004.
- Dhingra, K.; Fousková, P.; Angelovski, G.; Maier, M. E.; Logothetis, N. K.; Tóth, É. *J. Biol. Inorg. Chem.* **2008**, 13, 35.
- Mishra, A.; Fousková, P.; Angelovski, G.; Balogh, E.; Mishra, A. K.; Logothetis, N. K.; Tóth, É. *Inorg. Chem.* **2008**, 47, 1370.
- Angelovski, G.; Fousková, P.; Mamedov, I.; Canals, S.; Tóth, É.; Logothetis, N. K. *ChemBioChem* **2008**, 9, 1729.
- Dhingra, K.; Maier, M. E.; Beyerlein, M.; Angelovski, G.; Logothetis, N. K. *Chem. Commun.* **2008**, 3444.
- Ward, K. M.; Aletras, A. H.; Balaban, R. S. *J. Magn. Reson.* **2000**, 143, 79.
- Toth, E.; Helm, L.; Merbach, A.E. Metal complexes as MRI contrast enhancement agents. In *Comprehensive Coordination Chemistry II*; Elsevier: Amsterdam, 2004.
- Caravan, P.; Ellison, J. J.; McMurry, T. J.; Lauffer, R. B. *Chem. Rev.* **1999**, 99, 2293.
- Zhang, S.; Winter, P.; Wu, K.; Sherry, A. D. *J. Am. Chem. Soc.* **2001**, 123, 1517.
- Zhang, S.; Merritt, M.; Woessner, D. E.; Lenkinski, R. E.; Sherry, A. D. *Acc. Chem. Res.* **2003**, 36, 783.
- Woods, M.; Woessner, D. E.; Sherry, A. D. *Chem. Soc. Rev.* **2006**, 35, 500.
- Chauvin, T.; Durand, P.; Bernier, M.; Meudal, H.; Doan, B.-T.; Noury, F.; Badet, B.; Beloeil, J.-C.; Toth, E. *Angew. Chem., Int. Ed.* **2008**, 47, 4370.
- Yoo, B.; Pagel, M. D. *J. Am. Chem. Soc.* **2006**, 128, 14032.
- Zhang, S.; Trokowsky, R.; Sherry, A. D. *J. Am. Chem. Soc.* **2003**, 125, 15288.
- Ren, J.; Trokowsky, R.; Zhang, S.; Malloy, C. R.; Sherry, A. D. *Magn. Reson. Med.* **2008**, 60, 1047.
- Trokowsky, R.; Ren, J.; Kalman, F. K.; Sherry, A. D. *Angew. Chem., Int. Ed.* **2005**, 44, 6920.
- Aime, S.; Castelli, D. D.; Terreno, E. *Angew. Chem., Int. Ed.* **2002**, 41, 4334.
- Zhou, J.; van Zijl, P. C. M. *Prog. NMR Spectrosc.* **2006**, 48, 109.
- Li, A. X.; Wojciechowski, F.; Suchy, M.; Jones, C. K.; Hudson, R. H. E.; Menon, R. S.; Bartha, R. *Magn. Reson. Med.* **2006**, 59, 374.
- Pasha, A.; Lin, M.; Tircsó, G.; Rostollan, C. L.; Woods, M.; Kiefer, G. E.; Sherry, A. D.; Sun, X. *J. Biol. Inorg. Chem.* **2009**, 14, 421.
- Xu, R.; Wang, Y.; Wang, X.; Jeong, E.-K.; Parker, D. L.; Lu, Z. R. *Exp. Biol. Med.* **2007**, 232, 1081.
- Fanning, A. M.; Plush, S. E.; Gunnlaugsson, T. *Chem. Commun.* **2006**, 3791.
- Barge, A.; Tei, L.; Upadhyaya, D.; Fedeli, F.; Beltrami, L.; Stefania, R.; Aime, S.; Cravotto, G. *Org. Biomol. Chem.* **2008**, 6, 1176.
- Zhang, S.; Michaudet, L.; Burgess, S.; Sherry, A. D. *Angew. Chem., Int. Ed.* **2002**, 41, 1919.
- Zhang, S.; Kovacs, Z.; Burgess, S.; Aime, S.; Terreno, E.; Sherry, A. D. *Chem. Eur. J.* **2001**, 7, 288.
- Dunand, F. A.; Aime, S.; Merbach, A. E. *J. Am. Chem. Soc.* **2000**, 122, 1506.
- Ambrose, J.; Covington, A.; Thirsk, H. *Trans. Faraday Soc.* **1975**, 65, 1897.
- Schwarzenbach, G.; Kampitsch, E.; Steiner, R. *Helv. Chim. Acta* **1945**, 28, 1139.
- Kandel, E. R.; Schwartz, J. H.; Jessell, T. M., Eds., *Principles of Neural Science*, 4th ed.; McGraw-Hill, 2000.
- McMahon, M. T.; Gilad, A. A.; Zhou, J.; Sun, P. Z.; Bulte, J. W. M.; van Zijl, P. C. M. *Magn. Reson. Med.* **2006**, 55, 836.
- Terreno, E.; Castelli, D. D.; Cravotto, G.; Milone, L.; Aime, S. *Invest. Radiol.* **2004**, 39, 235.
- Aime, S.; Barge, A.; Della Castelli, D.; Fedeli, F.; Mortillaro, A.; Nielsen, F. U.; Terreno, E. *Magn. Reson. Med.* **2002**, 47, 639.
- Genik-Sas-Berezowsky, R. M.; Spinner, I. H. *Can. J. Chem.* **1970**, 48, 163.